iScience

CellPress
OPEN ACCESS

Article

gp78-regulated KAP1 phosphorylation induces radioresistance in breast cancer by facilitating PPP1CC/PPP2CA ubiquitination

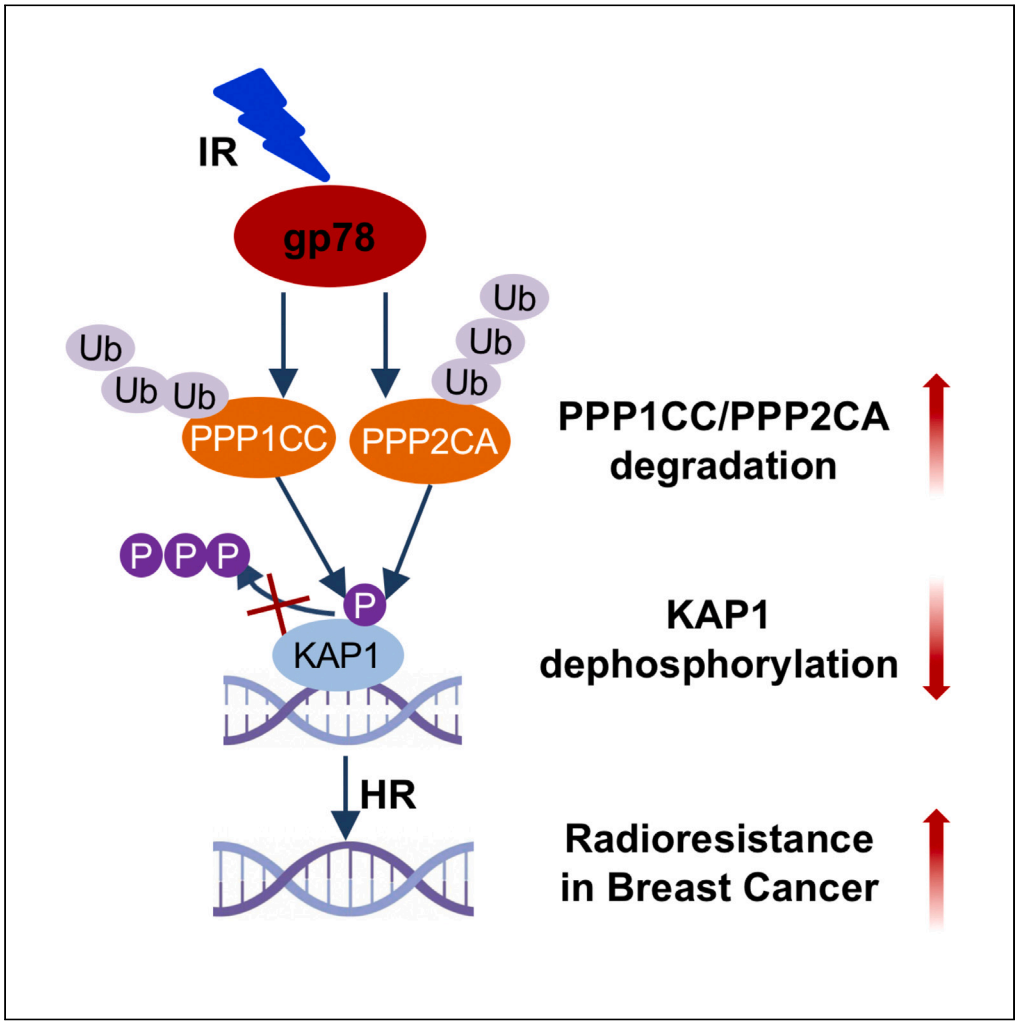

Yamei Han, Mingming Xiao, Shaorong Zhao, Han Wang, Rui Li, Bo Xu

xubo731@cqu.edu.cn

Highlights

gp78 enhances radiotherapy-induced DNA damage repair in breast cancer cells

gp78 modulates KAP1 phosphorylation through regulation of phosphatase degradation

gp78 is a potential biomarker for radioresistance in breast cancer

Han et al., iScience 27, 110847
September 20, 2024
https://doi.org/10.1016/j.isci.2024.110847

iScience

CellPress
OPEN ACCESS

Article

gp78-regulated KAP1 phosphorylation induces radioresistance in breast cancer by facilitating PPP1CC/PPP2CA ubiquitination

Yamei Han,[1,2,5] Mingming Xiao,[3,5] Shaorong Zhao,[2,5] Han Wang,[4] Rui Li,[1,2] and Bo Xu[1,2,4,6,*]

SUMMARY

Adjuvant radiation therapy is a common treatment for breast cancer, yet its effectiveness is often limited by radioresistance in patients. Identifying novel targets to combat this radioresistance is imperative. Recent investigations show that gp78 is upregulated in drug-resistant breast cancer cells. Our study reveals that gp78 markedly increased the phosphorylation of KAP1 and promoted DNA damage repair caused by ionizing radiation. Mechanistically, gp78 degrades phosphatases (PPP1CC/PPP2CA) in a ubiquitination-dependent manner. PPP1CC and PPP2CA are crucial regulators of KAP1 phosphorylation in response to DNA damage. Therefore, gp78 leads to a notable elevation in the phosphorylation of KAP1 by degrading phosphatases, thereby promoting the DNA damage repair process and increasing the radioresistance of tumor cells. The identification of gp78 as a pivotal regulator in radioresistance suggests a promising avenue for intervention. Combining blockade strategies targeting gp78 holds a significant potential for reversing radioresistance and improving the efficacy of breast cancer radiotherapy.

INTRODUCTION

Breast cancer, a prevalent type of cancer worldwide, affects women and, rarely, men.[1] Various factors elevate the risk of developing breast cancer, including age, a family history of breast cancer, specific gene mutations like BRCA1 and BRCA2, hormonal influences (such as early onset of menstruation, late menopause, hormone replacement therapy), obesity, alcohol consumption, and exposure to ionizing radiation (IR).[2–4] In the management of breast cancer, two commonly employed treatment modalities are radiotherapy and chemotherapy.[5] Radiotherapy utilizes high-energy radiation to eliminate cancer cells and reduce tumor size. By damaging the DNA within cancer cells, radiotherapy hinders the ability of these cells to divide and proliferate.[6] DDR (DNA damage response) is a pivotal factor in the resistance of tumor cells to DNA-damaging agents or radiation therapy during the tumor treatment process.[7] DDR is regulated by various posttranslational modifications (PTMs), including ubiquitination, deubiquitination, phosphorylation, and acetylation.[8–10] The ubiquitin-proteasome system is implicated in the expression or function of target proteins and is involved in various physiological and pathological processes of breast cancer.[11] Inhibitors targeting the 26S proteasome, when combined with other drugs, have demonstrated promising therapeutic outcome in clinical breast cancer treatment.[12] Therefore, a comprehensive understanding of the role of ubiquitination in breast cancer, identifying potential tumor promoters or suppressors, should be applied to the clinical treatment of breast cancer.

gp78, also known as autocrine motility factor receptor (AMFR), is a multifunctional protein that holds a central position in a variety of cellular processes, encompassing protein degradation and cellular signaling.[13] A clinical data study revealed a significant increase in gp78 expression in bladder carcinoma. The expression of gp78 showed a negative correlation with E-cadherin and a positive correlation with N-cadherin. This suggests that gp78 may play a role in regulating epithelial-mesenchymal transition.[14] In the context of breast cancer, gp78 performs multifaceted functions in disease development and progression.[15] It enhances cell migration, invasion, and metastasis by controlling the degradation of proteins involved in cell adhesion and extracellular matrix remodeling.[16] Additionally, gp78 has been implicated in drug resistance in breast cancer. The upregulation of gp78 has been observed in drug-resistant breast cancer cells, and gp78 can modulate the degradation of proteins associated with drug sensitivity.[17] However, the precise mechanisms underlying gp78-mediated chemotherapy resistance and radioresistance in breast cancer remain under investigation. Additional investigation is crucial to gain a thorough comprehension of the intricate molecular mechanisms involved.

[1]Department of Biochemistry and Molecular Biology, Tianjin Medical University Cancer Institute and Hospital, National Clinical Research Center for Cancer, Tianjin 300060, China
[2]Tianjin's Clinical Research Center for Cancer, Key Laboratory of Breast Cancer Prevention and Therapy, Tianjin Medical University, Ministry of Education, Key Laboratory of Cancer Prevention and Therapy, Tianjin 300060, China
[3]Department of Pancreatic Surgery, Fudan University Shanghai Cancer Center, Shanghai 200032, China
[4]Center for Intelligent Oncology, Chongqing University Cancer Hospital, Chongqing University School of Medicine, Chongqing 400030, China
[5]These authors contributed equally
[6]Lead contact
*Correspondence: xubo731@cqu.edu.cn
https://doi.org/10.1016/j.isci.2024.110847

To further elucidate the role of gp78 in radioresistance, *in vitro* and *in vivo* experiments reveal that gp78 promotes DNA damage repair and enhances radioresistance in breast cancer. As an E3 ubiquitin ligase, gp78 exerts its influence by promoting the degradation of targeting protein phosphatase 1 catalytic subunit gamma (PPP1CC) and protein phosphatase 2 catalytic subunit alpha isoform (PPP2CA), ultimately leading to a reduction in protein stability. Upon exposure to DNA-damaging agents, KAP1 (Krüppel-associated box [KRAB]-associated protein 1) phosphorylation is primarily mediated by ataxia telangiectasia mutated (ATM) and ATM- and Rad3-related (ATR) kinases.[18] Our results offer substantiating evidence for the regulatory role of PPP1CC and PPP2CA in KAP1 dephosphorylation, thereby suppressing the DNA damage repair and elucidating their involvement in mediating gp78's impact on KAP1. Collectively, these results offer invaluable molecular insights into how gp78 regulates the function of KAP1 during the DDR process. Moreover, our results suggest that targeting gp78 has the potential to overcome the radiotherapy resistance in breast cancer cells.

RESULTS

gp78 promotes the response to DNA damage induced by radiotherapy in breast cancer cells

An analysis of the TCGA database revealed that breast tumor tissue exhibits a high expression level of gp78 (Figure S1A). To investigate the function of gp78 in the DNA damage response in breast cancer, we measured the changes in the γH2AX level over time after exposure to 6 Gy ionizing radiation in MDA-MB-231 and SUM-159 cells. Radiation exposure significantly induced the formation of γH2AX, a DNA damage marker. Interestingly, overexpression of gp78 significantly promoted DNA damage repair and increased the phosphorylation of KAP1 (Figures 1A–1D). To evaluate the effect of gp78 on cellular radiosensitivity, colony formation assays were carried out with MDA-MB-231 cells that had been rendered stably overexpressing gp78. The western blot result showed the expression level of gp78 in stable cell lines (Figure S1B). The cells received irradiation at incremental doses, specifically 0 Gy, 2 Gy, 4 Gy, and 6 Gy. As illustrated in Figures 1E and 1F, overexpression of gp78 substantially enhanced the ability of the cells to form colonies, indicating increased radioresistance. To further confirm this observation, we conducted immunofluorescence staining to quantify the count of γH2AX foci in MDA-MB-231 cells stably expressing gp78. At 4, 8, and 24 h post-exposure to 6 Gy ionizing radiation, the gp78 overexpression notably reduced the count of γH2AX foci compared to the control group (Figures 1G and 1H). Ionizing-radiation-induced double-strand breaks (DSBs) can undergo repair through two primary pathways: homologous recombination (HR) and non-homologous end joining (NHEJ).[19] KAP1 promotes HR by facilitating the recruitment of HR factors to DNA damage sites.[20] To investigate which repair pathway gp78 is involved in, we conducted HR assays using stably transfected DR-GFP-U2OS cell lines. Our findings demonstrated a substantial enhancement in the capacity for homologous recombination (HR) repair due to the presence of gp78, suggesting the involvement of gp78 in HR repair pathways (Figure 1I). Additionally, By employing the comet assay, a method designed to detect DNA damage on a single-cell basis, we observed that gp78 significantly reduced the presence of tails (indicating damaged DNA) in MDA-MB-231 cells (Figures S1C and S1D). To further explore the influence of gp78 on the radiosensitivity of breast cancer cells, MDA-MB-231 cells that were stably overexpressing gp78 were subjected to a 6-Gy radiation exposure, and we subsequently evaluated cell viability using a CCK8 assay. Overexpression of gp78 significantly increased cell viability and increased radioresistance in response to radiation exposure (Figure S1E).

In conclusion, these results collectively suggest that gp78 enhances DNA damage repair, thereby playing a role in bolstering the resistance of breast cancer cells against DNA-damaging radiotherapy.

Knocking down gp78 enhances cellular radiosensitivity in breast cancer cells

To validate our findings, we performed knockdown experiments targeting gp78 in MDA-MB-231 cells and SUM-159 cells. The changes in the γH2AX level over time were measured following exposure to 6 Gy ionizing radiation. The results indicated that knocking down gp78 significantly delayed the DNA damage repair process, reduced the phosphorylation of KAP1, and increased the cytotoxicity of radiotherapy (Figures 2A–2D). We constructed stable cell lines, knocking down gp78 using the shRNA lentiviral to validate our findings, and we performed knockdown experiments targeting gp78 in MDA-MB-231 cells. The qPCR result confirmed the effective knockdown of gp78 (Figure S2A). To evaluate the effect of knocking down of gp78 on cellular radiosensitivity, colony formation assays were conducted with MDA-MB-231 cells stably knocking down gp78. The cells were subjected to irradiation at incremental doses, specifically 0 Gy, 2 Gy, 4 Gy, and 6 Gy. As illustrated in Figures 2E and 2F, knocking down gp78 reduced the ability of the cells to form colonies, indicating increased radiosensitivity. This observation was further confirmed through immunofluorescence staining to quantify the count of γH2AX foci. At 4, 8, and 24 h post-exposure to 6 Gy ionizing radiation, shgp78-1 and shgp78-2 increased the count of γH2AX foci compared to the control group (Figures 2G and 2H). To investigate whether gp78 is involved in DNA damage repair, HR assays were conducted using stably transfected DR-GFP-U2OS cell lines. We deleted endogenous gp78 using shRNA. As show in Figure 2I, gp78-knockdown DR-GFP-U2OS cells displayed defective HR compared to control shRNA cells, indicating that gp78 is necessary for HR activation. Additionally, comet assay revealed a significant delay in DNA repair in gp78 knocked down cells (Figures S2B and S2C). To further explore the influence of knockdown gp78 on the radiosensitivity of breast cancer cells, MDA-MB-231 cells stably knocking down gp78 were subjected to a 6 Gy radiation exposure, and cell viability was subsequently evaluated using a CCK8 assay. The knockdown of gp78 resulted in a substantial reduction in cell viability and an increase in the radiosensitivity of tumor cells (Figure S2D).

In conclusion, these results collectively suggest that reducing gp78 inhibits DNA damage repair and increases sensitivity to DNA-damaging radiotherapy.

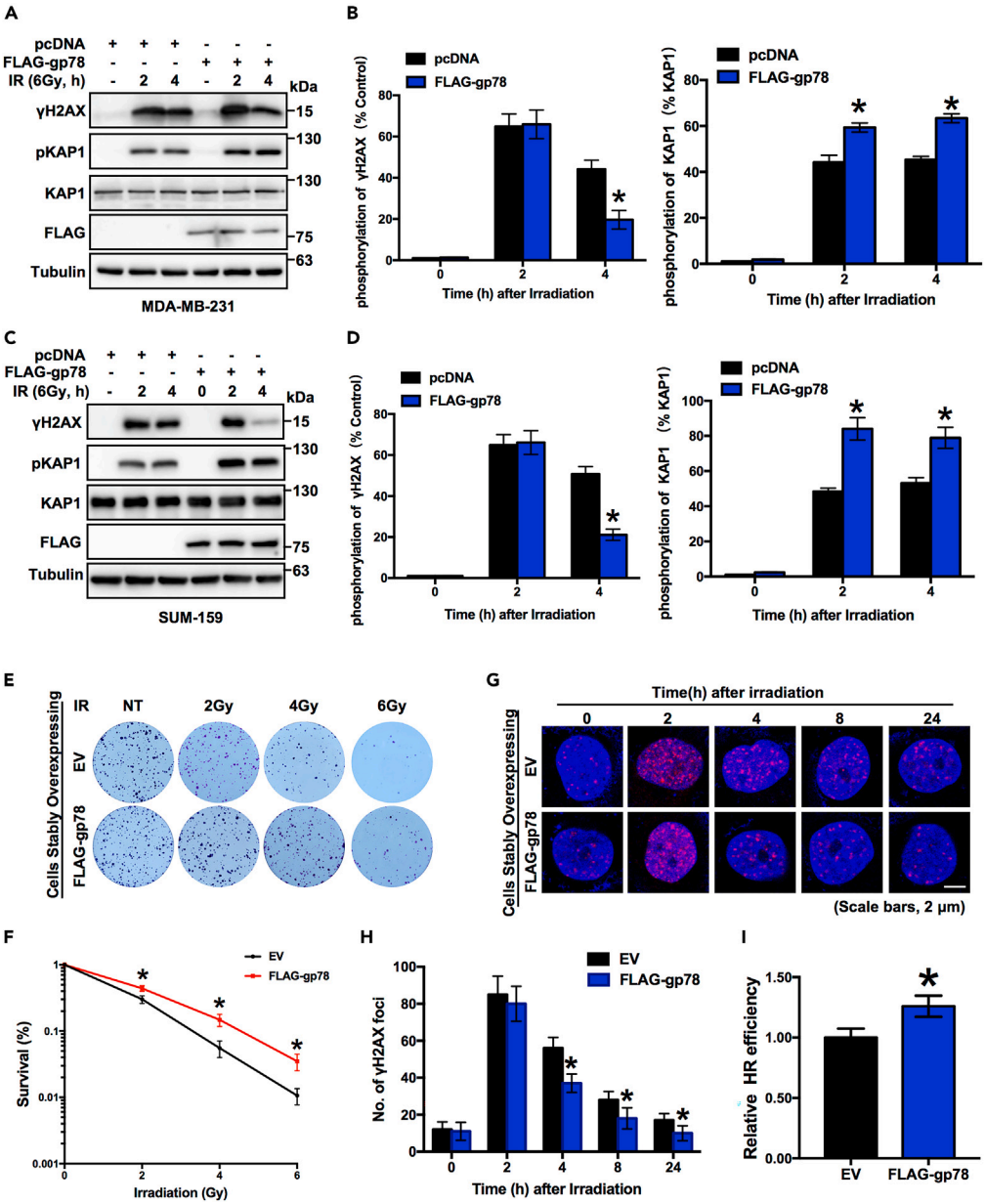

Figure 1. gp78 promotes DDR induced by radiotherapy in breast cancer cells

(A–D) Overexpression of gp78 promotes DNA damage response and increases the phosphorylation of KAP1. MDA-MB-231 cells (A and B) and SUM-159 cells (C and D) were transfected with pcDNA or FLAG-tagged gp78 for 24 h prior to exposure to 6 Gy ionizing radiation for 4 h. The data presented are representative of three independent experiments per cell line. The band intensities of immunoblots were quantified by ImageJ software. The data are presented as means ±SEMs; $n = 3$.

(E and F) gp78 increases the ability of cells to form colonies. The colony formation assay was conducted in control and gp78-overexpressing stable MDA-MB-231 cell lines after exposure to ionizing radiation (IR) at doses of 0, 2, 4, and 6 Gy. The results are presented as the averages of triplicate samples; data shown as means ± SEM.

(G and H) gp78 reduces γH2AX foci formation and promotes DNA damage response. Representative images of immunofluorescence staining of γH2AX foci (red) and nuclei (blue) in control and gp78-overexpressing stable MDA-MB-231 cell lines exposed to 6 Gy ionizing radiation for the indicated times. Nuclear γH2AX foci were quantified in 100 cells, and the results are presented as averages. Data represent one experiment of three independent experiments. Scale bar, 2 μm.

(I) gp78 significantly enhances the HR repair ability. HR efficiency was examined in U2OS reporter cells. The DR-GFP-U2OS cell line was transfected with control or FLAG-gp78 plasmid for 24 h and then transfected with I-SceI plasmid to induce DNA damage. GFP-positive cells were quantified by flow cytometry. The results are presented as the averages of triplicate samples. Data are presented as means ± SEM, unpaired two-tailed Student's t test, *$p < 0.05$, vs. EV.

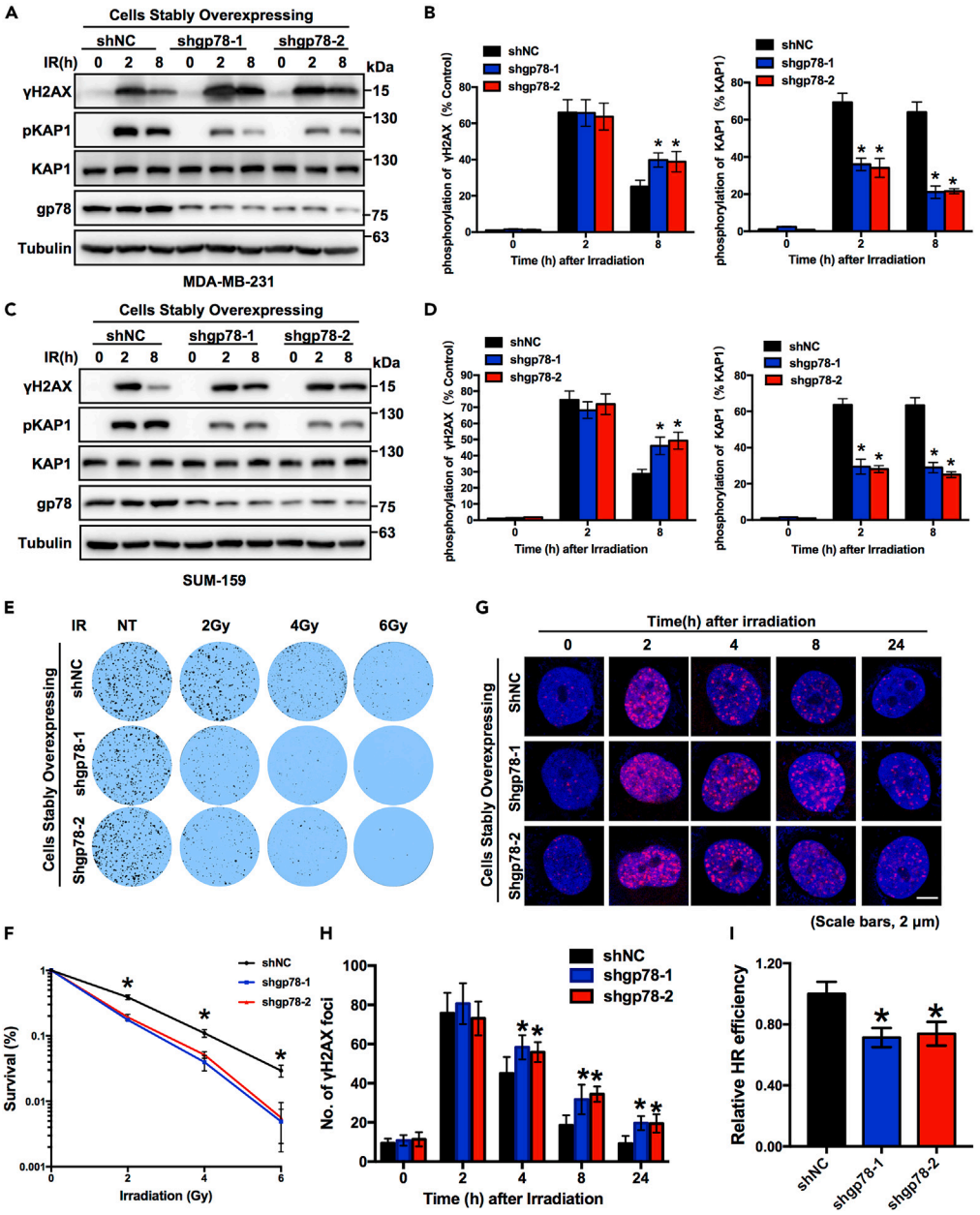

Figure 2. Knocking down gp78 induces radiosensitivity in breast cancer cells

(A–D) Knockdown of gp78 induces radiosensitivity and decreases the phosphorylation of KAP1. MDA-MB-231 cells (A and B) and SUM-159 cells (C and D) were stably transfected with shNC, shgp78-1, or shgp78-2 to exposure to 6 Gy ionizing radiation for 8 h. Data are representative of three independent experiments per cell line. The data are representative of three independent experiments per cell line. The band intensities of immunoblots were quantified by ImageJ software. The data are presented as means ±SEMs; $n = 3$.

(E and F) Knocking down gp78 reduces the ability of the cells to form colonies. The colony formation assay was conducted in shNC, shgp78-1, or shgp78-2 stable MDA-MB-231 cell lines after exposure to ionizing radiation (IR) at doses of 0, 2, 4, and 6 Gy. The results are presented as the averages of triplicate samples; data shown as means ± SEM.

(G and H) Knocking down gp78 increases γH2AX foci formation and delays DNA damage repair. Representative images of immunofluorescence staining of γH2AX foci (red) and nuclei (blue) in shNC, shgp78-1, or shgp78-2 stable MDA-MB-231 cell lines exposed to 6 Gy ionizing radiation for the indicated times. Nuclear γH2AX foci were quantified in 100 cells, and the results are presented as averages. Data represent one experiment of three independent experiments. Scale bar, 2 μm.

(I) Knocking down gp78 significantly reduces the HR repair ability. HR efficiency was examined in U2OS reporter cells. The DR-GFP-U2OS cell line was treated with shNC, shgp78-1, or shgp78-2 plasmid for 24 h and then transfected with I-SceI plasmid to induce DNA damage. GFP-positive cells were quantified by flow cytometry. The results are presented as the averages of triplicate samples. Data are presented as means ± SEM, unpaired two-tailed Student's t test, *$p < 0.05$, vs. shNC.

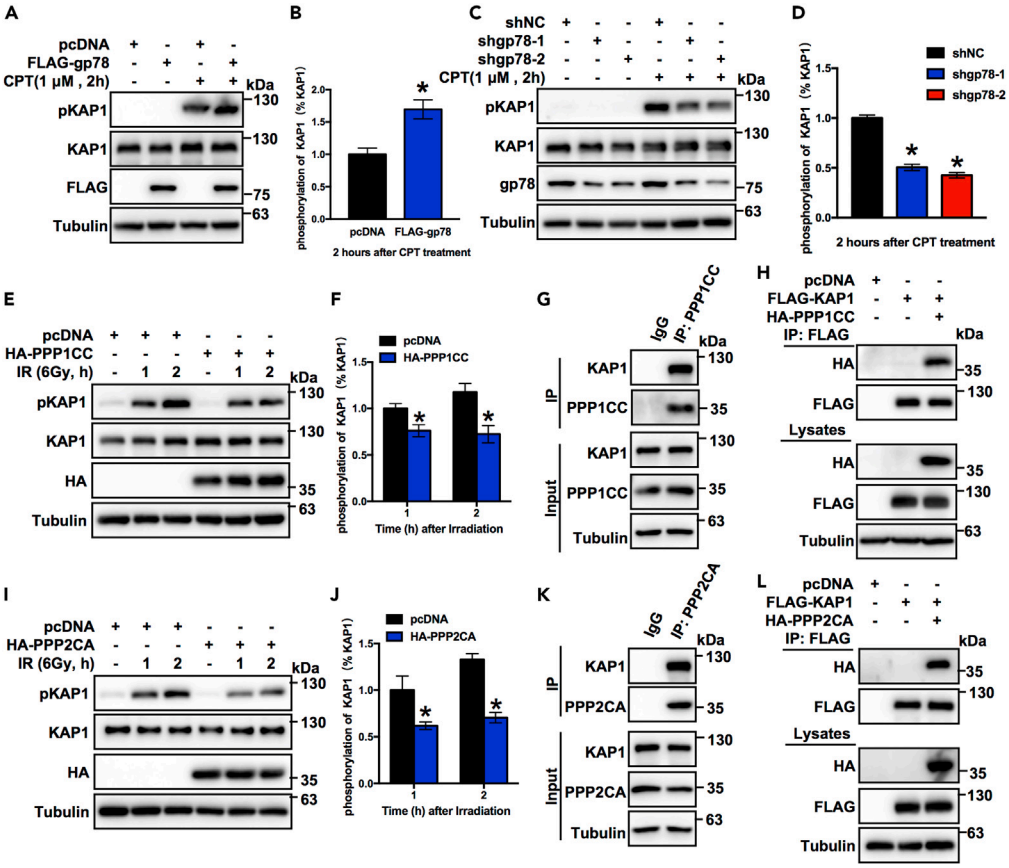

Figure 3. PPP1CC and PPP2CA are phosphatases of KAP1

(A and B) Overexpression of gp78 increases the phosphorylation of KAP1. MDA-MB-231 cells were transfected with pcDNA or FLAG-tagged gp78 for 24 h and then treated with CPT for 2 h. Immunoblots were conducted, and the band intensities were quantified by ImageJ software. Results represent one experiment of three independent experiments.

(C and D) The phosphorylation of KAP1 is reduced upon gp78 knockdown. MDA-MB-231 cells were transfected with shNC, shgp78-1, or shgp78-2 for 24 h and then treated with CPT for 2 h. Immunoblots were conducted, and the band intensities were quantified by ImageJ software. Results represent one experiment of three independent experiments.

(E and F) PPP1CC dephosphorylates KAP1. MDA-MB-231 cells were transfected with pcDNA or HA-PPP1CC for 24 h and then treated with 6 Gy ionizing radiation for 2 h. Immunoblots were conducted, and the band intensities were quantified by ImageJ software. Results represent one experiment of three independent experiments.

(G) Endogenous PPP1CC interacts with KAP1. Immunoblots of MDA-MB-231 cell lysates subjected to Co-IP with an anti-PPP1CC antibody or anti-rabbit IgG and protein A/G Sepharose beads, then immunoblotted with the indicated antibodies. Results represent one experiment of three independent experiments.

(H) KAP1 interacts with PPP1CC. HA-PPP1CC was cotransfected with FLAG-KAP1 into MDA-MB-231 cells. Cell lysates were incubated with an anti-FLAG antibody and protein A/G Sepharose beads. The precipitates and lysates were individually subjected to immunoblotting with the indicated antibodies. Results represent one experiment of three independent experiments.

(I and J) PPP2CA dephosphorylates KAP1. MDA-MB-231 cells were transfected with pcDNA or HA-PPP2CA for 24 h and then treated with 6 Gy ionizing radiation for 2 h. Immunoblots were conducted, and the band intensities were quantified by ImageJ software. Results represent one experiment of three independent experiments.

(K) Endogenous PPP2CA interacts with KAP1. Immunoblots of MDA-MB-231 cell lysates subjected to IP with an anti-PPP2CA antibody or anti-rabbit IgG and protein A/G Sepharose beads, and then immunoblotted with the indicated antibodies. Results represent one experiment of three independent experiments.

(L) KAP1 is a target of PPP2CA. HA-PPP2CA was cotransfected with FLAG-KAP1 into MDA-MB-231 cells. Cell lysates were incubated with an anti-FLAG antibody and protein A/G Sepharose beads. The precipitates and lysates were individually subjected to immunoblotting with the indicated antibodies. Results represent one experiment of three independent experiments. Data are presented as means ± SEM, unpaired two-tailed Student's t test, *$p < 0.05$, vs. pcDNA.

gp78 regulates KAP1 phosphorylation through the phosphatase pathway

CPT is an inhibitor of DNA topoisomerase 1 that induces double-stranded DNA breaks.[21] To investigate whether gp78 can regulate the phosphorylation of KAP1 under CPT treatment. MDA-MB-231 cells were subjected to transfection with FLAG-tagged gp78, followed by treatment with or without CPT. As shown in Figures 3A and 3B, the presence of CPT resulted in increased phosphorylation of KAP1. Strikingly, overexpression of gp78 significantly increased the phosphorylation of KAP1, whereas knockdown of gp78 by shRNA decreased KAP1

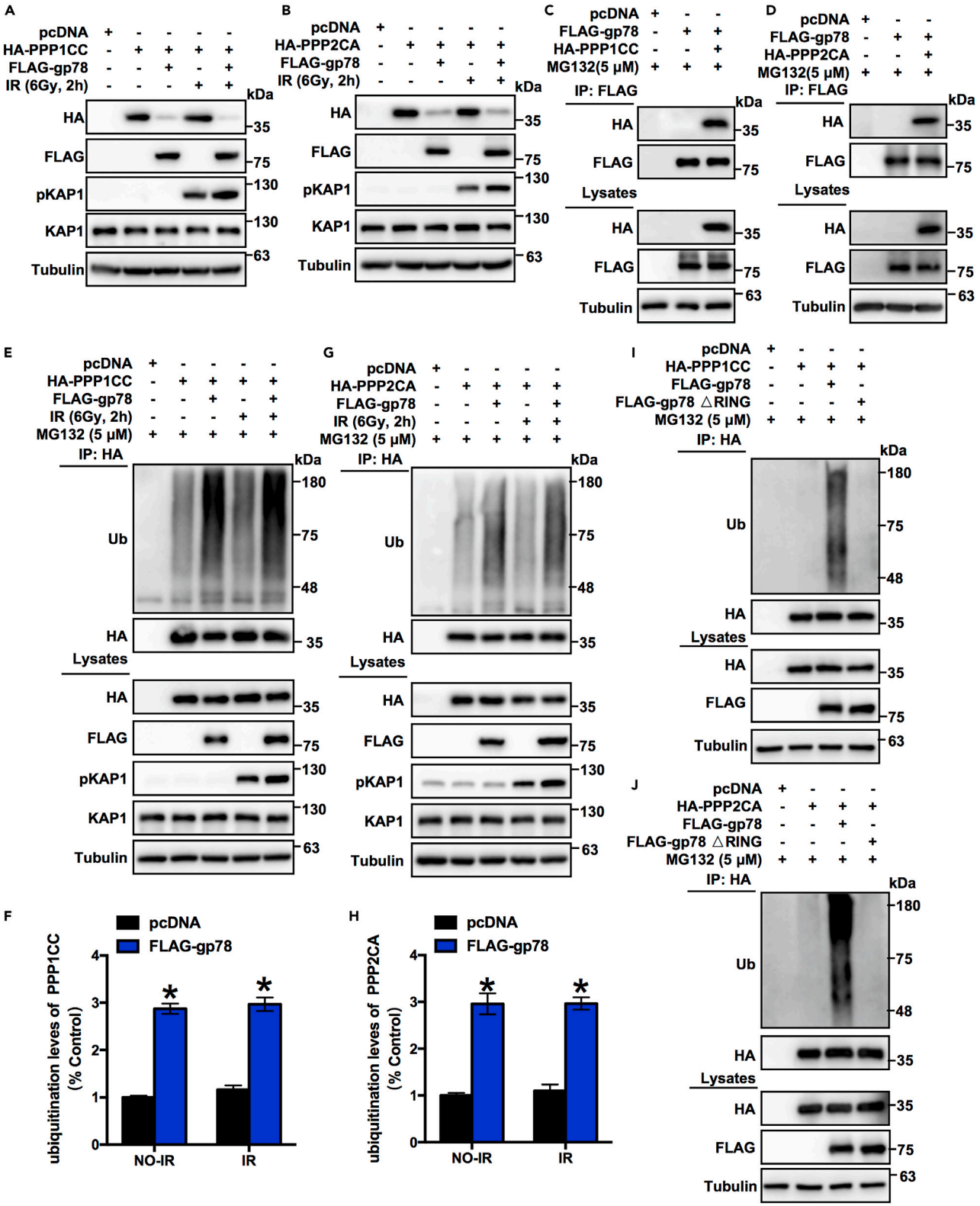

Figure 4. gp78 is the E3 ligase of both phosphatase PPP1CC and PPP2CA

(A and B) gp78 reduces the protein levels of both PPP1CC (A) and PPP2CA (B). HA-PPP1CC or HA-PPP2CA was cotransfected with FLAG-gp78, and the transfected cells were then treated with 6 Gy ionizing radiation. Results represent one experiment of three independent experiments.

Figure 4. *Continued*

(C and D) gp78 associates with PPP1CC and PPP2CA. HA-PPP1CC or HA-PPP2CA was cotransfected with FLAG-gp78 into MDA-MB-231 cells for 48 h. Cell lysates were incubated with an anti-FLAG antibody and protein A/G Sepharose beads. The precipitates and lysates were individually subjected to immunoblotting with the indicated antibodies. Results represent one experiment of three independent experiments.

(E–H) gp78 increases the ubiquitination levels of PPP1CC and PPP2CA. Plasmids encoding HA-tagged PPP1CC (E) or PPP2CA (F) were cotransfected with FLAG-gp78 prior to treatment with 5 μM MG132 for 8 h. Cell lysates were incubated with an anti-HA antibody and protein A/G Sepharose beads. The precipitates and lysates were individually subjected to immunoblotting with the indicated antibodies. Immunoblots were conducted, and the band intensities were quantified by ImageJ software. Results represent one experiment of three independent experiments.

(I and J) The degradation of PPP1CC and PPP2CA by gp78 depend on the RING finger domain. Plasmids encoding HA-tagged PPP1CC (I) or PPP2CA (J) were cotransfected with FLAG-gp78 or FLAG-gp78 ΔRING prior to treatment with 5 μM MG132 for 8 h. Cell lysates were incubated with an anti-HA antibody and protein A/G Sepharose beads. The precipitates and lysates were individually subjected to immunoblotting with the indicated antibodies. Data are presented as means ± SEM, $n = 3$, unpaired two-tailed Student's t test, $^*p < 0.05$, vs. pcDNA.

phosphorylation (Figures 3C and 3D). Notably, the phosphorylation of KAP1 was affected by gp78. As an E3 ubiquitin ligase, gp78 cannot directly impact protein phosphorylation. Furthermore, coimmunoprecipitation (Co-IP) analysis revealed no interaction between gp78 and KAP1. To identify the target protein of gp78 that regulates KAP1 phosphorylation, we conducted an analysis using liquid chromatography–tandem mass spectrometry (LC-MS/MS), which identified several putative target proteins, including the phosphatases PPP1CC and PPP2CA (Figures S3A and S3B). We hypothesized that PPP1CC and PPP2CA might dephosphorylate KAP1. To assess this hypothesis, MDA-MB-231 cells were transfected with HA-tagged PPP1CC plasmid, followed by exposure to ionizing radiation or control conditions. Remarkably, overexpression of PPP1CC reduced the phosphorylation of KAP1 (Figures 3E and 3F). The interaction between PPP1CC and KAP1 was validated through endogenous Co-IP conducted in MDA-MB-231 cells and SUM-159 cells (Figures 3G and S3C). Furthermore, Co-IP analysis provided confirmation of the interaction between HA-tagged PPP1CC and FLAG-tagged KAP1 within MDA-MB-231 cells (Figure 3H). These findings indicate an interaction between PPP1CC and KAP1, facilitating its dephosphorylation. Furthermore, to explore whether PPP2CA also regulates KAP1 phosphorylation, MDA-MB-231 cells were transfected with HA-tagged PPP2CA plasmid, followed by exposure to ionizing radiation or control conditions. Consistent with the findings for PPP1CC, overexpression of PPP2CA significantly reduced the phosphorylation of KAP1 (Figures 3I and 3J). Endogenous Co-IP showed that PPP2CA also interacts with KAP1 in MDA-MB-231 cells and SUM-159 cells (Figures 3K and S3D). Furthermore, Co-IP analysis provided confirmation of the interaction between HA-tagged PPP2CA and FLAG-tagged KAP1 within MDA-MB-231 cells (Figure 3L). In summary, these data collectively suggest that PPP1CC and PPP2CA are sufficient to regulate KAP1 phosphorylation by PTM.

gp78 associates with and ubiquitinates PPP1CC and PPP2CA

We hypothesized that gp78 might ubiquitinate PPP1CC and PPP2CA. To investigate this hypothesis, MDA-MB-231 cells were overexpressed with PPP1CC and PPP2CA, either in the presence or in the absence of gp78. Treatment with gp78 resulted in a noteworthy decrease in the protein levels of PPP1CC and PPP2CA (Figures 4A and 4B), whereas mRNA levels of PPP1CC and PPP2CA showed no significant change (Figures S4A and S4B). As shown in Figure S4C, overexpression of gp78 also caused a profound reduction in the endogenous PPP1CC and PPP2CA protein levels in MDA-MB-231 cells and SUM-159 cells. Moreover, the utilization of shRNA to knock down gp78 resulted in an elevation of protein levels for endogenous PPP1CC and PPP2CA (Figure S4D). Next, to test the hypothesis that gp78 is the E3 ligase for PPP1CC and PPP2CA, Co-IP analysis was carried out. As show in Figures 4C and 4D, HA-tagged PPP1CC or HA-tagged PPP2CA was coexpressed with FLAG-tagged gp78. The interaction between PPP1CC/PPP2CA and gp78 was also confirmed by endogenous Co-IP in MDA-MB-231 cells and SUM-159 cells, establishing PPP1CC and PPP2CA interact with gp78 (Figures S4E–S4G). As an E3 ubiquitin ligase, gp78 reduces the protein levels of both PPP1CC and PPP2CA. Our hypothesis postulated that gp78 might modulate the protein levels of PPP1CC and PPP2CA via the ubiquitin-proteasome pathway (UPP) of protein degradation. To test this hypothesis, we conducted transfections of MDA-MB-231 cells involving HA-tagged PPP1CC and PPP2CA, both in the presence and in the absence of FLAG-tagged gp78. The presence of gp78 led to the ubiquitination of PPP1CC and PPP2CA (Figures 4E–4H). gp78 contains a RING finger domain endowed with E3 activity.[22] To investigate the involvement of the RING finger domain in the degradation of phosphatases PPP1CC and PPP2CA, we assessed the impact of gp78 RING mutants on the ubiquitination levels of PPP1CC and PPP2CA. Upon transfecting the gp78 RING-finger-deficient mutant instead of wild-type gp78, a significant reduction in the protein ubiquitination levels of PPP1CC and PPP2CA was observed (Figures 4I and 4J). This implies that the ability of gp78 to target phosphatases for degradation requires the RING finger domain, further indicating that gp78 mediates the ubiquitination degradation pathway of phosphatases. To further clarify the function of gp78 RING finger domain in the DNA damage response, we measured the changes of γH2AX level over time after exposure to 6 Gy ionizing radiation in MDA-MB-231 and SUM-159 cells. Consistent with our findings, overexpression of gp78 RING-finger-deficient mutant had no effect on DNA damage repair or the phosphorylation of KAP1 (Figures S4H and S4I). Furthermore, gp78 RING-finger-deficient mutant did not affect the ability of the cells to form colonies, indicating gp78 RING finger domain regulates DNA damage repair (Figures S4H–S4K). In summary, these data indicate that gp78 functions as the E3 ligase for both PPP1CC and PPP2CA, influencing DNA damage repair through the ubiquitination pathway.

gp78 regulates the degradation of PPP1CC and PPP2CA and inhibits the interaction between phosphatases and KAP1

We further investigated whether gp78 regulates the degradation of PPP1CC and PPP2CA. MDA-MB-231 cells that had been rendered stably expressing either shNC, shgp78-1, or shgp78-1 were subjected to transfection with HA-tagged PPP1CC and exposed to CHX, which is an

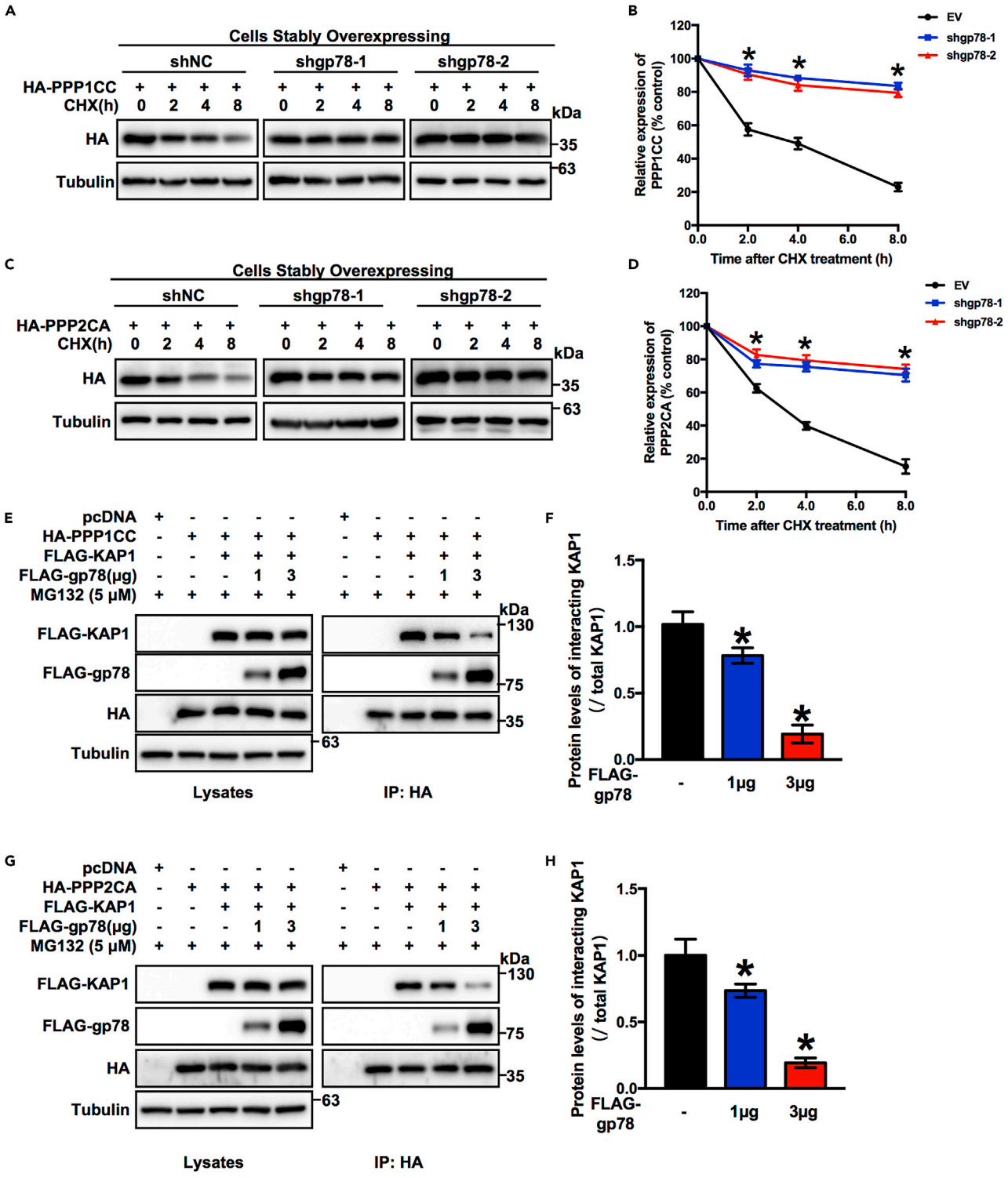

Figure 5. gp78 reduces the stability of PPP1CC and PPP2CA

(A and B) gp78 knockdown reduces the degradation rate of PPP1CC. MDA-MB-231 cells stably expressing shNC, shgp78-1, or shgp78-2 were transfected with HA-PPP1CC for 24 h and then incubated in medium containing 100 ng/mL CHX for the indicated time. Immunoblots were conducted, and the band intensities were quantified by ImageJ software. Results represent one experiment of three independent experiments. The data are presented as the means ± SEMs; $n = 3$.

Figure 5. *Continued*

(C and D) gp78 knockdown reduces the degradation rate of PPP2CA. MDA-MB-231 cells stably expressing shNC, shgp78-1, or shgp78-2 were transfected with HA-PPP2CA for 24 h and then incubated in medium containing 100 ng/mL CHX for the indicated time. Immunoblots were conducted, and the band intensities were quantified by ImageJ software. Results represent one experiment of three independent experiments. The data are presented as means ±SEMs; $n = 3$.

(E–H) gp78 inhibits the interaction between KAP1 and PPP1CC or PPP2CA and is dose dependent. HA-tagged PPP1CC (E) or PPP2CA (G) was cotransfected with FLAG-KAP1, and FLAG-gp78 was subsequently transfected for 48 h and treated with 5 μM MG132 for 8 h. Cell lysates were incubated with an anti-HA antibody and purified with protein A/G Sepharose beads. The precipitates and lysates were individually subjected to immunoblotting with the indicated antibodies. Immunoblots were conducted, and the band intensities were quantified by ImageJ software. Results represent one experiment of three independent experiments. Data are presented as means ± SEM, $n = 3$, unpaired two-tailed Student's t test, $^*p < 0.05$, vs. pcDNA.

inhibitor of eukaryotic protein synthesis, to determine the half-life of PPP1CC. Knockdown of gp78 significantly reduced the proteasome-mediated degradation of PPP1CC, resulting in an extended half-life (Figures 5A and 5B). We conducted a similar experiment to examine the impact of gp78 on the degradation of PPP2CA. Knockdown of gp78 decreased the degradation rate of PPP2CA and prolonged its half-life (Figures 5C and 5D). We further examined the impact of gp78 on the stability of endogenous PPP1CC and PPP2CA proteins. As shown in Figures S5A and S5B, knockdown of gp78 decreased the degradation rate of endogenous PPP1CC and PPP2CA. Additionally, Co-IP analysis assay revealed that overexpression of gp78 disrupted the interaction between PPP1CC or PPP2CA and KAP1 in a dose-dependent manner (Figures 5E–5H). Conversely, immunofluorescence assay and co-IP show that knockdown of gp78 increased the interaction between PPP1CC or PPP2CA and KAP1 in SUM-159 cells (Figures S5C–S5F). In conclusion, these data collectively establish gp78 as the E3 ligase for both PPP1CC and PPP2CA, attenuating the interaction between PPP1CC or PPP2CA and KAP1 and thereby regulating the phosphorylation of KAP1.

PPP1CC and PPP2CA delay the DNA damage repair process induced by radiotherapy in breast cancer cells

To explore the involvement of PPP1CC and PPP2CA in the DNA damage response within the context of breast cancer, we monitored the alteration in the γH2AX level over a defined period following exposure to 6 Gy ionizing radiation in MDA-MB-231 cells and SUM-159 cells. Overexpression of PPP1CC and PPP2CA significantly delayed the DNA damage repair process, reduced the phosphorylation of KAP1, and increased the cytotoxicity of radiotherapy (Figures 6A–6D). To evaluate the effect of PPP1CC and PPP2CA on cellular radiosensitivity, colony formation assays were carried out with MDA-MB-231 cells that had been rendered stably overexpressing PPP1CC and PPP2CA. The result revealed that PPP1CC and PPP2CA significantly reduce the ability of cells to form colonies and increase radiosensitivity (Figures 6E and 6F). Immunofluorescence staining of γH2AX foci further confirmed a significant reduction in the number of foci at 4, 8, and 24 h after exposure to 6 Gy ionizing radiation when PPP1CC and PPP2CA were stably overexpressed (Figures 6G and 6H). Moreover, HR assays demonstrated that PPP1CC and PPP2CA significantly inhibited the HR repair ability (Figure 6I). Furthermore, comet assays indicated that PPP1CC and PPP2CA significantly increased the tail length (indicating DNA damage) in MDA-MB-231 cells (Figures S6A and S6B). In summary, these results suggest that PPP1CC and PPP2CA delay DNA damage repair and increase sensitivity to DNA-damaging radiotherapy, mediating the regulatory effect of gp78 on KAP1.

gp78 increases radioresistance in breast cancer cells

To further explore the influence of gp78 on the radiosensitivity of breast cancer cells, we further validated our results through *in vivo* experiments. We established a xenograft model using stable gp78-knockout MDA-MB-231 cells and control cells to observe and measure the changes in tumor volume over time. After statistical analysis, we found that the growth rate and weight of the gp78-knockout tumors were not significantly different from the control group (Figures S7A–S7D). These results suggest that knocking down gp78 expression has no effect on tumor growth. We established xenograft models using cells with gp78 knockout and examined the effect of gp78 knockout on radiosensitivity. Following a 15-day incubation period, the xenografts were subjected to a therapeutic regimen consisting of a cumulative radiation dose of 12 Gy, administered at a daily rate of 4 Gy (on days 15, 16, and 17). Following irradiation with 12 Gy, the sizes of the xenograft tumors were assessed every 3 days over a 32-day period. On day 32, the xenograft tumors were harvested for analysis. Through statistical analysis, our observations revealed that the tumors lacking gp78 exhibited a notably slower growth rate, and their weight was significantly reduced following irradiation (Figures 7A–7D). The levels of γH2AX in xenograft tumors were increased significantly upon gp78 knockdown, whereas Ki67 levels significantly decreased, as confirmed by immunohistochemical analysis of xenograft tumor sections (Figures 7E and 7F). Overall, these results imply that gp78 increases radioresistance in breast cancer cells.

DISCUSSION

This research underscores the significance of gp78 in promoting radioresistance in breast cancer by disrupting the interactions between phosphatases and KAP1. We observed upregulation of gp78 expression in breast cancer patients. Interestingly, we discovered that the novel involvement of PPP1CC and PPP2CA phosphatases in dephosphorylating KAP1 during DNA damage response. Additionally, gp78, which functions as an E3 ubiquitin ligase for PPP1CC and PPP2CA, increases their ubiquitination and accelerates their degradation. Consequently, gp78 modulates KAP1 phosphorylation by regulating the degradation of phosphatases, thereby influencing breast cancer cells' sensitivity to the DNA damage response post-radiotherapy. In conclusion, our phenotypic and mechanistic studies strongly support the crucial role of gp78 in mediating radioresistance in breast cancer cells (Figure S7E).

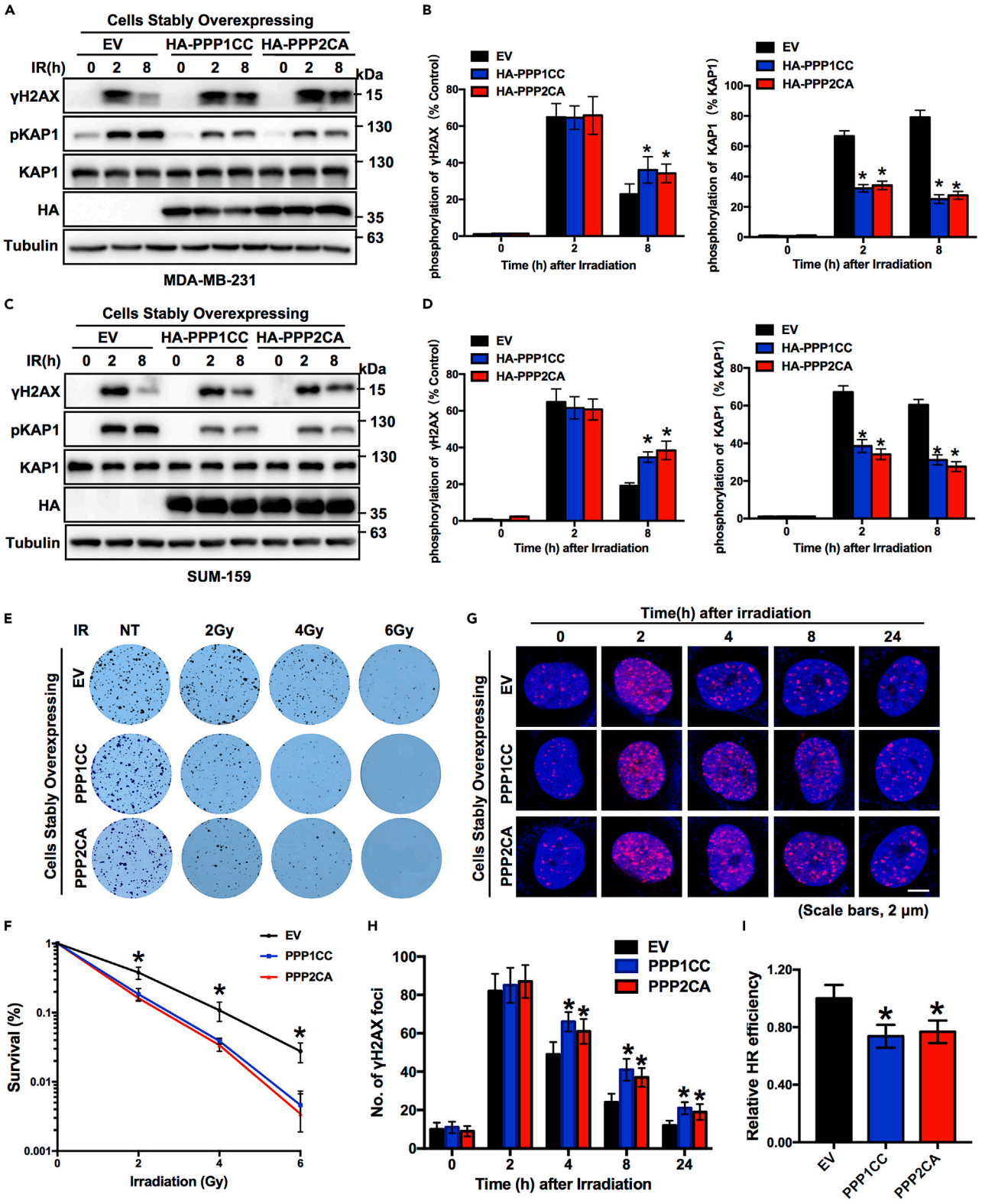
A
Cells Stably Overexpressing
EV
HA-PPP1CC
HA-PPP2CA
IR(h) 0 2 8 0 2 8 0 2 8
kDa
γH2AX
pKAP1
KAP1
HA
Tubulin
15
130
130
35
63
MDA-MB-231
B
EV
HA-PPP1CC
HA-PPP2CA
phosphorylation of γH2AX (% Control)
Time (h) after Irradiation
phosphorylation of KAP1 (% KAP1)
C
SUM-159
D
E
IR
NT
2Gy
4Gy
6Gy
Cells Stably Overexpressing
EV
PPP1CC
PPP2CA
F
Survival (%)
Irradiation (Gy)
G
Time(h) after irradiation
0
2
4
8
24
(Scale bars, 2 μm)
H
No. of γH2AX foci
I
Relative HR efficiency

Figure 6. PPP1CC and PPP2CA reduce the DDR induced by radiotherapy in breast cancer cells

(A–D) PPP1CC and PPP2CA delay DNA damage response and reduce the phosphorylation of KAP1. MDA-MB-231 cells (A) and SUM-159 cells (C) were transfected with pcDNA or HA-tagged PPP1CC or PPP2CA for 24 h prior to exposure to 6 Gy ionizing radiation for 8 h. The data presented are representative of three independent experiments per cell line.

(E and F) PPP1CC and PPP2CA reduce the ability of cells to form colonies. Colony formation assay in control, PPP1CC-overexpressing, and PPP2CA-overexpressing stable MDA-MB-231 cell lines after exposure to ionizing radiation at doses of 0, 2, 4, and 6 Gy. The data presented are representative of three independent experiments, and the results are presented as the averages of triplicate samples; data shown as mean ± SEM.

(G and H) PPP1CC and PPP2CA increase γH2AX foci formation and promote DNA damage response. Representative images of immunofluorescence staining of γH2AX foci (red) and nuclei (blue) in MDA-MB-231 cells (control or gp78-overexpressing) exposed to IR (6 Gy) for the indicated time. Nuclear γH2AX foci formation was quantified in 100 cells, and data are presented as averages. The data presented are representative of three independent experiments. Scale bar, 2 μm.

(I) PPP1CC and PPP2CA reduced the HR repair ability. HR efficiency was assessed in U2OS reporter cells. The DR-GFP-U2OS cell line was treated with control, HA-PPP1CC, or HA-PPP2CA plasmid for 24 h and then transfected with I-SceI plasmid to induce DNA damage. GFP-positive cells were quantified using flow cytometry. The results are presented as the averages of triplicate samples. Data are presented as means ± SEM, unpaired two-tailed Student's t test, $*p < 0.05$, vs. EV.

Previous studies have also reported high expression levels of gp78 in various cancer types. One important finding is that gp78 may promote the DNA damage response. Elevated levels of gp78 have been associated with unfavorable outcomes in breast cancer, affecting cell-cycle regulation, metabolism, receptor-mediated signaling, and cellular stress response pathways.[15] Recent studies have suggested that gp78-mediated degradation of TMCO1 controls tumor growth and drug resistance.[17] Additionally, gp78 enhances sarcoma metastasis through the degradation of KAI1.[23] However, the mechanisms underlying gp78-mediated chemoresistance and radioresistance in breast cancer are still being investigated. To explore the role of gp78 in the DNA damage response, we utilized both gain-of-function and loss-of-function methods. γH2AX levels were monitored over time after exposure to 6 Gy ionizing radiation, and the results revealed that gp78 significantly promoted DNA damage response (Figures 1A–1D and 2A–2D). Colony formation assays and comet assays demonstrated that gp78 substantially increased the colony-forming ability of cells, indicating increased radioresistance (Figures 1E, 1F, 2E, and 2F). Furthermore, we validated the regulatory effect of gp78 on the DNA damage response using a tumorigenesis assay in nude mice. The findings indicated that the knockdown of gp78 resulted in a significant increase in the sensitivity of mouse tumors to radiotherapy and a substantial decrease in the rate of tumor growth (Figure 7). Through both *in vivo* and *in vitro* experiments, we demonstrate that gp78 enhances the DNA damage response process and elevates radioresistance.

In order to unravel the mechanism through which gp78 governs DNA damage response, we conducted western blot analysis to screen for DNA-damage-related proteins. Interestingly, we observed that gp78 increased the phosphorylation of KAP1 in response to DNA damage (Figures 3A–3C). However, additional Co-IP experiments did not validate an interaction between KAP1 and gp78 (data not shown). To identify potential target proteins of gp78, we performed LC−MS/MS analysis, which revealed PPP1CC and PPP2CA as putative candidates (Figures S3A and S3B).

PP1 and PP2 are serine/threonine phosphatases known for their high conservation and crucial involvement in governing various cellular processes.[24,25] These phosphatases are essential players in the DNA damage response, a process crucial for maintaining genomic stability.[26,27] For instance, Wip1 (also known as PPM1D), a DDR phosphatase, plays a role in dephosphorylating γH2AX, thereby attenuating the DNA damage response.[28] Phosphatases function as primary regulators of DDR signaling by dephosphorylating key signal transducing kinases, such as ATM and ATR, as well as DDR substrates, including H2AX, KAP1, and p53.[29–31] PPP1CC represents one of the catalytic subunits of protein phosphatase 1 (PP1), whereas PPP2CA functions as the catalytic subunit of protein phosphatase 2 (PP2). These two phosphatases, PPP1CC and PPP2CA, are involved in diverse cellular processes, including but not limited to cell-cycle regulation, signal transduction, metabolism, and the neuronal DNA damage response.[30,31] In our study, we discovered that both PPP1CC and PPP2CA can inhibit the phosphorylation of KAP1 during the DDR process (Figures 3E, 3F, 3I, and 3J). Co-IP experiments demonstrated that the phosphatases PPP1CC and PPP2CA interact with KAP1 (Figures 3G, 3H, 3K, and 3L). Additionally, phenotypic experiments further confirmed that PPP1CC and PPP2CA delay the DNA damage repair process and increase cellular radiosensitivity (Figures 6 and S6). Therefore, phosphatases, acting as intermediate proteins, may mediate the interaction between gp78 and KAP1.

gp78, a protein with diverse cellular functions, is involved in processes such as protein quality control, cell migration and invasion, EMT, and drug resistance.[13] To gain a deeper understanding of its molecular mechanism, we conducted experiments that revealed gp78's function as an E3 ligase, facilitating the proteasomal degradation of PPP1CC and PPP2CA (Figure 4). Protein degradation assays indicated that knockdown of gp78 significantly decreased the degradation rates of PPP1CC and PPP2CA, leading to an increased protein half-life (Figures 5A–5D, S5A, and S5B). Additionally, Co-IP showed that overexpression of gp78 significantly decreased the interactions between KAP1 and the phosphatases PPP1CC and PPP2CA, and knockdown gp78 significantly increased the interactions between KAP1 and the phosphatases PPP1CC and PPP2CA (Figures 5E–5H and S5C–S5F). These findings provide evidence that gp78 promotes the degradation of PPP1CC and PPP2CA through ubiquitination, thereby inhibiting the dephosphorylation of KAP1 during DNA damage response.

In conclusion, this study elucidates a biochemical mechanism through which gp78 regulates the DNA damage response. Through degradation of phosphatases PPP1CC and PPP2CA, gp78 promotes the phosphorylation of KAP1, thereby promoting the DNA damage response process. Inhibiting gp78 activity through pharmacological or genetic approaches may offer a new therapeutic strategy to improve radiosensitivity during breast cancer radiotherapy.

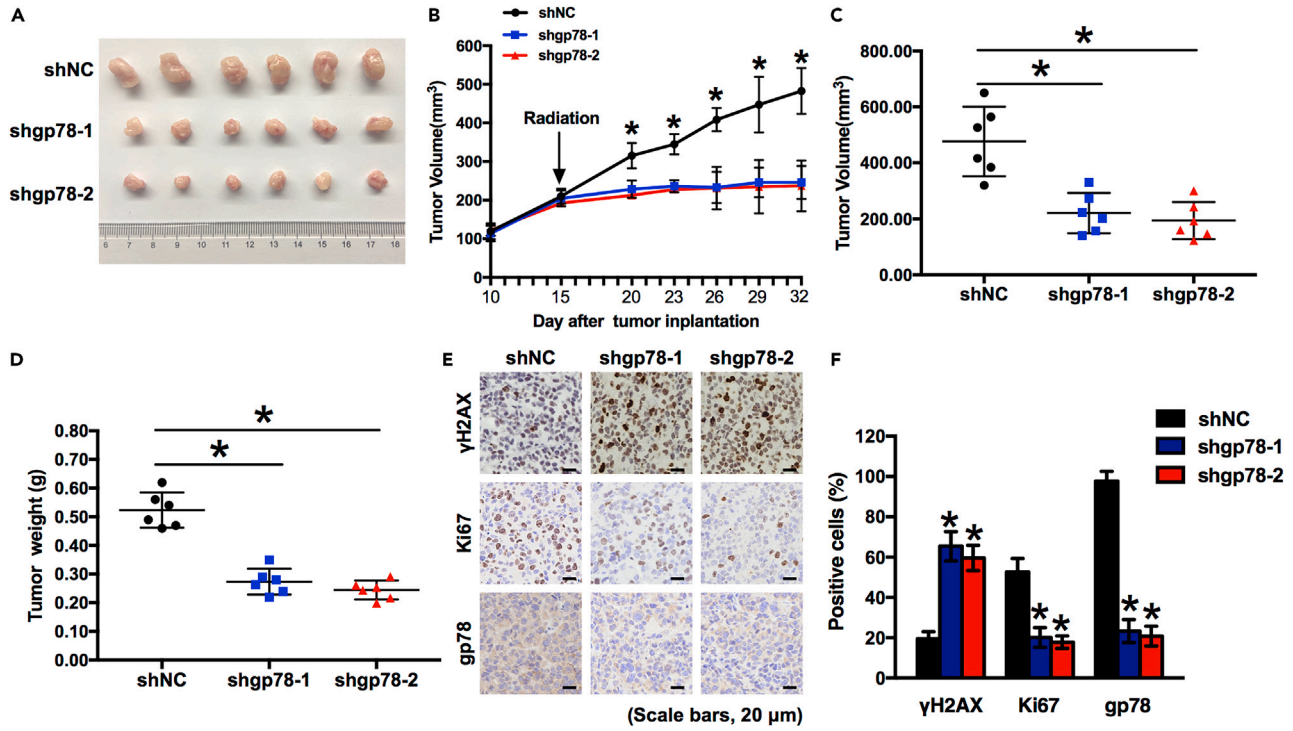

Figure 7. gp78 knockdown enhances radiosensitivity *in vivo*

(A–D) BALB/c nu/nu mice bearing MDA-MB-231 xenografts. Xenograft tumors were formed from MDA-MB-231 cells stably transfected with shNC, shgp78-1, or shgp78-2 (n = 6 mice per group). Tumor growth curves in xenograft mice are presented, and tumor volumes were measured every 3 days after exposure to ionizing radiation.

(C and D) Tumor volume and weight at the endpoint of the subcutaneous xenograft assay.

(E and F) Representative immunohistochemical staining of the xenograft tumor sections with γH2AX, Ki67, and gp78 and the quantification. Scale bar, 20 μm. Data are presented as means ± SEM, n = 6, unpaired two-tailed Student's t test, *$p < 0.05$, vs. shNC.

Limitations of the study

Although we provide important discoveries revealed in our study, there are still some limitations. Firstly, there are no clinic studies to validate our conclusions. If conditions permit, we will further investigate the expression level of gp78 in clinical samples before and after radiotherapy. Secondly, the role of gp78 was further validated by *in vivo* experiments with gp78 conditional knockout mice. Thirdly, our findings show gp78 regulates the DNA damage response. gp78 is also associated with cell metabolism, and whether the metabolic state of the cell will be altered after DDR needs to be further explored.

RESOURCE AVAILABILITY

Lead contact

Further information and request for resources and reagents should be directed to and will be fulfilled by the lead contact, Dr Bo Xu (xubo731@cqu.edu.cn).

Materials availability

This study did not create any novel research reagents.

Data and code availability

- The mass spectrometry proteomics data have been deposited to the ProteomeXchange Consortium (https://proteomecentral.proteomexchange.org) via the iProX partner repository with the dataset identifier PXD054846.
- Data: the data generated in this study are available upon request from the lead contact.
- Code: this paper does not report original code.
- Any additional information required to reanalyze the data reported in this paper is available from the lead contact upon request.

ACKNOWLEDGMENTS

This work was supported by the National Natural Science Foundation of China (Grant Nos. 82003237, 82203438, and 82403769).

AUTHOR CONTRIBUTIONS

Y.H., M.X., S.Z., and B.X. contributed to design the experiments of this study. Y.H., M.X., S.Z., H.W., and RL. contributed to conduct the experiments, data analysis, and discussion of the result. B.X., Y.H., and R.L. obtained the funding. All authors contributed to the writing and editing of the manuscript.

DECLARATION OF INTERESTS

The authors declare that they have no competing interests.

STAR★METHODS

Detailed methods are provided in the online version of this paper and include the following:

- KEY RESOURCES TABLE
- EXPERIMENTAL MODEL AND STUDY PARTICIPANT DETAILS
  - Cell lines and cell treatment
  - Animals experiments
- METHOD DETAILS
  - Western blot and coimmunoprecipitation (Co-IP)
  - Cell proliferation and colony formation assays
  - Plasmids and transfection
  - Immunofluorescence analysis
  - Immunohistochemical analysis
  - Ionizing radiation
  - Comet assay
  - HR reporter assay
  - LC–MS/MS analysis
- QUANTIFICATION AND STATISTICAL ANALYSIS

SUPPLEMENTAL INFORMATION

Supplemental information can be found online at https://doi.org/10.1016/j.isci.2024.110847.

Received: November 3, 2023
Revised: March 15, 2024
Accepted: August 27, 2024
Published: August 30, 2024

REFERENCES

1. Sung, H., Ferlay, J., Siegel, R.L., Laversanne, M., Soerjomataram, I., Jemal, A., and Bray, F. (2021). Global Cancer Statistics 2020: GLOBOCAN Estimates of Incidence and Mortality Worldwide for 36 Cancers in 185 Countries. CA. Cancer J. Clin. *71*, 209–249.
2. Carbine, N.E., Lostumbo, L., Wallace, J., and Ko, H. (2018). Risk-reducing mastectomy for the prevention of primary breast cancer. Cochrane Database Syst. Rev. *4*, Cd002748.
3. Barchiesi, G., Mazzotta, M., Krasniqi, E., Pizzuti, L., Marinelli, D., Capomolla, E., Sergi, D., Amodio, A., Natoli, C., Gamucci, T., et al. (2020). Neoadjuvant Endocrine Therapy in Breast Cancer: Current Knowledge and Future Perspectives. Int. J. Mol. Sci. *21*, 3528.
4. Picon-Ruiz, M., Morata-Tarifa, C., Valle-Goffin, J.J., Friedman, E.R., and Slingerland, J.M. (2017). Obesity and adverse breast cancer risk and outcome: Mechanistic insights and strategies for intervention. CA. Cancer J. Clin. *67*, 378–397.
5. Dent, R., Hanna, W.M., Trudeau, M., Rawlinson, E., Sun, P., and Narod, S.A. (2009). Pattern of metastatic spread in triple-negative breast cancer. Breast Cancer Res. Treat. *115*, 423–428.
6. He, M.Y., Rancoule, C., Rehailia-Blanchard, A., Espenel, S., Trone, J.C., Bernichon, E., Guillaume, E., Vallard, A., and Magné, N. (2018). Radiotherapy in triple-negative breast cancer: Current situation and upcoming strategies. Crit. Rev. Oncol. Hematol. *131*, 96–101.
7. Stover, E.H., Konstantinopoulos, P.A., Matulonis, U.A., and Swisher, E.M. (2016). Biomarkers of Response and Resistance to DNA Repair Targeted Therapies. Clin. Cancer Res. *22*, 5651–5660.
8. Liu, W., Zheng, M., Zhang, R., Jiang, Q., Du, G., Wu, Y., Yang, C., Li, F., Li, W., Wang, L., et al. (2023). RNF126-Mediated MRE11 Ubiquitination Activates the DNA Damage Response and Confers Resistance of Triple-Negative Breast Cancer to Radiotherapy. Adv. Sci. *10*, e2203884.
9. Zhang, F.L., Yang, S.Y., Liao, L., Zhang, T.M., Zhang, Y.L., Hu, S.Y., Deng, L., Huang, M.Y., Andriani, L., Ma, X.Y., et al. (2023). Dynamic SUMOylation of MORC2 orchestrates chromatin remodelling and DNA repair in response to DNA damage and drives chemoresistance in breast cancer. Theranostics *13*, 973–990.
10. Li, J., Zhao, H., McMahon, A., and Yan, S. (2022). APE1 assembles biomolecular condensates to promote the ATR-Chk1 DNA damage response in nucleolus. Nucleic Acids Res. *50*, 10503–10525.
11. Han, D., Wang, L., Jiang, S., and Yang, Q. (2023). The ubiquitin-proteasome system in breast cancer. Trends Mol. Med. *29*, 599–621.
12. Chen, D., Frezza, M., Schmitt, S., Kanwar, J., and Dou, Q.P. (2011). Bortezomib as the first proteasome inhibitor anticancer drug: current status and future perspectives. Curr. Cancer Drug Targets *11*, 239–253.
13. Joshi, V., Upadhyay, A., Kumar, A., and Mishra, A. (2017). Gp78 E3 Ubiquitin Ligase: Essential Functions and Contributions in Proteostasis. Front. Cell. Neurosci. *11*, 259.
14. Otto, T., Birchmeier, W., Schmidt, U., Hinke, A., Schipper, J., Rübben, H., and Raz, A. (1994). Inverse relation of E-cadherin and autocrine motility factor receptor expression as a prognostic factor in patients with bladder carcinomas. Cancer Res. *54*, 3120–3123.
15. Singhal, S.K., Byun, J.S., Yan, T., Yancey, R., Caban, A., Gil Hernandez, S., Bufford, S., Hewitt, S.M., Winfield, J., Pradhan, J., et al. (2022). Protein expression of the gp78 E3 ligase predicts poor breast cancer outcome based on race. JCI Insight *7*, e157465.
16. Xu, T., Yu, W., Fang, H., Wang, Z., Chi, Z., Guo, X., Jiang, D., Zhang, K., Chen, S., Li, M., et al. (2022). Ubiquitination of NLRP3 by gp78/Insig-1 restrains NLRP3 inflammasome activation. Cell Death Differ. *29*, 1582–1595.
17. Zheng, S., Zhao, D., Hou, G., Zhao, S., Zhang, W., Wang, X., Li, L., Lin, L., Tang, T.S., and Hu, Y. (2022). iASPP suppresses Gp78-mediated TMCO1 degradation to maintain Ca(2+) homeostasis and control tumor growth and drug resistance. Proc. Natl. Acad. Sci. USA *119*, e2111380119.
18. Zhou, J., Lim, C.U., Li, J.J., Cai, L., and Zhang, Y. (2006). The role of NBS1 in the modulation of PIKK family proteins ATM and ATR in the cellular response to DNA damage. Cancer Lett. *243*, 9–15.

19. Santivasi, W.L., and Xia, F. (2014). Ionizing radiation-induced DNA damage, response, and repair. Antioxid. Redox Signal. *21*, 251–259.
20. Ziv, Y., Bielopolski, D., Galanty, Y., Lukas, C., Taya, Y., Schultz, D.C., Lukas, J., Bekker-Jensen, S., Bartek, J., and Shiloh, Y. (2006). Chromatin relaxation in response to DNA double-strand breaks is modulated by a novel ATM- and KAP-1 dependent pathway. Nat. Cell Biol. *8*, 870–876.
21. Khaiwa, N., Maarouf, N.R., Darwish, M.H., Alhamad, D.W.M., Sebastian, A., Hamad, M., Omar, H.A., Orive, G., and Al-Tel, T.H. (2021). Camptothecin's journey from discovery to WHO Essential Medicine: Fifty years of promise. Eur. J. Med. Chem. *223*, 113639.
22. Ballar, P., Ors, A.U., Yang, H., and Fang, S. (2010). Differential regulation of CFTRDeltaF508 degradation by ubiquitin ligases gp78 and Hrd1. Int. J. Biochem. Cell Biol. *42*, 167–173.
23. Tsai, Y.C., Mendoza, A., Mariano, J.M., Zhou, M., Kostova, Z., Chen, B., Veenstra, T., Hewitt, S.M., Helman, L.J., Khanna, C., and Weissman, A.M. (2007). The ubiquitin ligase gp78 promotes sarcoma metastasis by targeting KAI1 for degradation. Nat. Med. *13*, 1504–1509.
24. Bollen, M., Peti, W., Ragusa, M.J., and Beullens, M. (2010). The extended PP1 toolkit: designed to create specificity. Trends Biochem. Sci. *35*, 450–458.
25. Morita, K., He, S., Nowak, R.P., Wang, J., Zimmerman, M.W., Fu, C., Durbin, A.D., Martel, M.W., Prutsch, N., Gray, N.S., et al. (2020). Allosteric Activators of Protein Phosphatase 2A Display Broad Antitumor Activity Mediated by Dephosphorylation of MYBL2. Cell *181*, 702–715.e20.
26. Ramos, F., Villoria, M.T., Alonso-Rodríguez, E., and Clemente-Blanco, A. (2019). Role of protein phosphatases PP1, PP2A, PP4 and Cdc14 in the DNA damage response. Cell Stress *3*, 70–85.
27. Zheng, X.F., Kalev, P., and Chowdhury, D. (2015). Emerging role of protein phosphatases changes the landscape of phospho-signaling in DNA damage response. DNA Repair *32*, 58–65.
28. Cha, H., Lowe, J.M., Li, H., Lee, J.S., Belova, G.I., Bulavin, D.V., and Fornace, A.J., Jr. (2010). Wip1 directly dephosphorylates gamma-H2AX and attenuates the DNA damage response. Cancer Res. *70*, 4112–4122.
29. Oleson, B.J., Naatz, A., Proudfoot, S.C., Yeo, C.T., and Corbett, J.A. (2018). Role of Protein Phosphatase 1 and Inhibitor of Protein Phosphatase 1 in Nitric Oxide-Dependent Inhibition of the DNA Damage Response in Pancreatic β-Cells. Diabetes *67*, 898–910.
30. Lee, D.H., and Chowdhury, D. (2011). What goes on must come off: phosphatases gate-crash the DNA damage response. Trends Biochem. Sci. *36*, 569–577.
31. Freeman, A.K., and Monteiro, A.N. (2010). Phosphatases in the cellular response to DNA damage. Cell Commun. Signal. *8*, 27.
32. Han, Y., Hu, Z., Cui, A., Liu, Z., Ma, F., Xue, Y., Liu, Y., Zhang, F., Zhao, Z., Yu, Y., et al. (2019). Post-translational regulation of lipogenesis via AMPK-dependent phosphorylation of insulin-induced gene. Nat. Commun. *10*, 623.
33. Hu, Z., Han, Y., Liu, Y., Zhao, Z., Ma, F., Cui, A., Zhang, F., Liu, Z., Xue, Y., Bai, J., et al. (2020). CREBZF as a Key Regulator of STAT3 Pathway in the Control of Liver Regeneration in Mice. Hepatology (Baltimore, Md) *71*, 1421–1436.
34. Xiao, M., Zhang, S., Liu, Z., Mo, Y., Wang, H., Zhao, X., Yang, X., Boohaker, R.J., Chen, Y., Han, Y., et al. (2022). Dual-functional significance of ATM-mediated phosphorylation of spindle assembly checkpoint component Bub3 in mitosis and the DNA damage response. J. Biol. Chem. *298*, 101632.

STAR★METHODS

KEY RESOURCES TABLE

REAGENT or RESOURCE	SOURCE	IDENTIFIER
Antibodies		
Rabbit monoclonal anti-phospho-Histone H2A.X (Ser139) antibody	Cell Signaling Technology	Cat# 9718; RRID: AB_2118009
Rabbit monoclonal anti-phospho-KAP-1 (Ser824) antibody	Cell Signaling Technology	Cat# 4127; RRID: AB_2209906
Rabbit monoclonal anti-KAP1 antibody	Cell Signaling Technology	Cat# 4123; RRID: AB_330970
Rabbit Polyclonal anti-gp78 antibody	Proteintech	Cat# 16675; RRID: AB_2226463
Rabbit Polyclonal anti-PPP1CC antibody	Proteintech	Cat# 11082; RRID: AB_2168085
Rabbit Polyclonal anti-PPP2CA antibody	Proteintech	Cat# 13482; RRID: AB_2169485
Rabbit polyclonal anti-Ub antibody	Proteintech	Cat# 10201; RRID: AB_2923727
Mouse monoclonal anti-HA antibody	Proteintech	Cat# 66006; RRID: AB_3086564
Rabbit polyclonal anti-Ki67 antibody	Proteintech	Cat# 27309; RRID: AB_2919649
Mouse polyclonal anti-Tubulin antibody	Proteintech	Cat# 11224; RRID: AB_2210206
Mouse monoclonal anti-FLAG M2 antibody	Sigma-Aldrich	Cat# F1804; RRID: AB_262044
Mouse monoclonal anti-His-probe (H-3) antibody	Santa Cruz	Cat# sc-8036; RRID: AB_627727
Alexa Fluor 488 goat anti-mouse IgG antibody	Thermo Fisher	Cat# A-11001; RRID: AB_2534069)
Alexa Fluor 594 goat anti-rabbit IgG antibody	Thermo Fisher	Cat# A-11012; RRID: AB_2534079
HRP-conjugated goat anti-rabbit IgG antibody	Jackson ImmunoResearch	Cat# 111-035-003; RRID: AB_2313567
HRP-conjugated goat anti-mouse IgG antibody	Jackson ImmunoResearch	Cat# 115-035-003; RRID:AB_10015289
Bacterial and virus strains		
DH5α	TIANGEN BIOTECH	Cat# CB101
Chemicals, peptides, and recombinant proteins		
ProLong® Gold antifade reagent with DAPI	Invitrogen	Cat# P36935
Lipofectamine™ 2000 Transfection Reagent	Thermo Fisher	Cat# 11668019
Puromycin dihydrochlorid	MCE	Cat# HY-B1743A
Camptothecin (CPT)	MCE	Cat# HY-16560
MG-132	MCE	Cat# HY-13259
Cycloheximide (CHX)	MCE	Cat# HY-12320
Opti-MEM® Reduced Serum Medium	Invitrogen	Cat# 11058-021
Trypsin-EDTA (0.25%), phenol red	Invitrogen	Cat# 25200072
DMEM, high glucose, no phosphates	Thermo Fisher	Cat# 11971025
Fetal Bovine Serum	Gibco	Cat# 16000044
Phosphatase inhibitor cocktail	Beyotime	Cat# P1082
TRIzol	Invitrogen	Cat# 15596018
PrimeScript™ RT Master Mix	Takara	Cat# RR036A
Hieff® qPCR SYBR Green Master Mix	Yeasen Biotechnology	Cat# 11201ES03
Immobilon-P (PVDF)	Merck Millipore	Cat# IPVH00010
Cell Counting Kit-8 (CCK-8)	Selleck	Cat# B34304
Pierce™ ChIP -GRADE PROTEIN A/G	Thermo Fisher	Cat# 26162
Protease and phosphatase inhibitor cocktail	Beyotime	Cat# P1046

(*Continued on next page*)

Continued

REAGENT or RESOURCE	SOURCE	IDENTIFIER
Critical commercial assays		
KOD-Plus-Neo Polymerase	TOYOBO	Cat# KOD-401
BCA protein assay Kit	Beyotime	Cat# P0009
Comet Assay	Trevigen	Cat# 4250-050-K
Experimental models: Cell lines		
Human: HEK293T cells	Cell Bank of the Chinese Academy of Sciences	N/A
Human: MDA-MB-231 cells cells	Cell Bank of the Chinese Academy of Sciences	N/A
Human: SUM-159 cells	Cell Bank of the Chinese Academy of Sciences	N/A
Human: U2OS DR-GFP	Laboratory of Jeremy Stark	N/A
Experimental models: Organisms/strains		
Mouse: BALB/c nu/nu	Beijing Experimental Animal Center	N/A
Oligonucleotides		
Primer: PPP1CC Forward: CCATGAATGTGCCAGCATCA	This paper	N/A
Primer: PPP1CC Reverse: AGTTGGTCGCATAATTCGCC	This paper	N/A
Primer: PPP2CA Forward: CGCATCACCATTCTTCGAGG	This paper	N/A
Primer: PPP2CA Reverse: AAGATCTGCCCATCCACCAA	This paper	N/A
Primer: gp78 Forward: TTGGTGGCTAAGCTCATCCA	This paper	N/A
Primer: gp78 Reverse: CGATCCTTGCAGAGCTGAAC	This paper	N/A
Primer: β-actin Forward: GATGAGATTGGCATGGCTTT	This paper	N/A
Primer: β-actin Reverse: GTCACCTTCACCGTTCCAGT	This paper	N/A
Primer shgp78-1: AACATCTGGTTATCCATGGCC	This paper	N/A
Primer shgp78-2: AATCGTGTCAGGGAAGAACAT	This paper	N/A
Recombinant DNA		
pLV3-EnCMV-AMFR-3×FLAG	MiaoLing Plasmid Platform	P54697
pLV3-CMV-PPP2CA-3×HA-Puro	MiaoLing Plasmid Platform	P63157
pLV3-CMV-PPP1CC-3×HA-Puro	MiaoLing Plasmid Platform	P57142
pLV3-EnCMV-AMFRΔRING -3×FLAG	MiaoLing Plasmid Platform	N/A
pCMV-FLAG-KAP1	This paper	N/A
His-KAP1	This paper	N/A
ISceI	This paper	N/A
pLV3-U6-gp78-shRNA1	This paper	N/A
pLV3-U6-gp78-shRNA2	This paper	N/A
pLVshRNA-EGFP(2A)	MiaoLing Plasmid Platform	P0648
Software and algorithms		
GraphPad Prism 8.0	GraphPad Software	https://www.graphpad.com
ImageJ	National Institutes of Health	https://imagej.nih.gov/ij/

EXPERIMENTAL MODEL AND STUDY PARTICIPANT DETAILS

Cell lines and cell treatment

MDA-MB-231 cells and SUM-159 cells were procured from the Cell Bank of the Chinese Academy of Sciences in Shanghai, China, and were cultured under controlled conditions, being kept in a humidified environment at 37°C with 5% CO2 for maintenance. The medium employed consisted of DMEM including 10% fetal bovine serum (FBS) (Gibco, CA), 100 units/ml penicillin, and 100 μg/ml streptomycin (Gibco, CA). Cells underwent trypsinization and were subjected to passaging at 2-day intervals. To initiate DNA damage, cells underwent plasmid transfection for 24 hours before being subjected to ionizing radiation at a dose of 6 Gy. For drug treatments, cells were initially transfected with a plasmid for 24 hours, followed by subsequent treatment with either 1 μM camptothecin (CPT, HY-16560, MCE), 5 μM MG132 (HY-13259, MCE) for an 8-hour duration, or 100 μM cycloheximide (CHX, HY-12320, MCE).

Animals experiments

In the context of the *in vivo* experiments, we employed female BALB/c nu/nu mice aged four weeks, which were procured from the Beijing Experimental Animal Center. All procedures involving animals were conducted in strict accordance with the guidelines and regulations established by the Institutional Animal Care and Use Committee of Tianjin Medical University Cancer Institute and Hospital, ensuring complete adherence to national standards. To initiate the experiments, cells were introduced by injection into the right thigh regions of the nude mice. Following a 15-day incubation period, the xenografts underwent a therapeutic regimen involving a cumulative radiation dose of 12 Gy, delivered at a daily rate of 4 Gy (on days 15, 16 and 17). After treating the xenograft tumors with 12 Gy irradiation, tumor sizes were monitored every 3 days over a 32-day period. The xenograft tumors were collected on day 32 for analysis. The ethical approval number for animal experiments is NSFC-AE-2020079.

METHOD DETAILS

Western blot and coimmunoprecipitation (Co-IP)

Western blot analysis was conducted following a protocol as previously documented.[32] In summary, cells were lysed on ice utilizing lysis buffer lysis buffer from Beyotime Biotechnology, which was augmented with both protease and phosphatase inhibitors, also sourced from Beyotime Biotechnology. Following cell lysis, after sonication of the cells, place them on ice for 30min. And then, the cell lysate underwent centrifugation at 16,000 × g for 10 minutes at 4°C, and the supernatant that ensued was employed for the purpose of immunoblot analysis.

In the Co-IP, the lysate derived from cells, which contained the overexpression of recombinant protein underwent an overnight incubation at 4°C with specific antibodies and was subsequently mixed with protein A/G Sepharose beads. Subsequently, the beads were subjected to three consecutive washes using cold lysis buffer.

Cell proliferation and colony formation assays

To perform the cell proliferation assay, cells were placed into unoccupied 96 well cell culture dishes, and cell proliferation was assessed through the introduction of CCK8 reagent at 0, 24, 48, and 96 hours. The colony formation assay was performed following irradiation. Stable MDA-MB-231 cells were cultivated over a span of 14 days, after which the colonies were fixed and subjected to staining with crystal violet. Surviving clones were defined as colonies containing over 50 cells, and the colony count was adjusted based on plating efficiency.

Plasmids and transfection

All plasmids were validated through DNA sequencing. The transfection of plasmids into cells was conducted using Lipofectamine 2000 (Life Technologies) in accordance with the manufacturer's instructions.

Immunofluorescence analysis

Immunofluorescence analysis was conducted following a protocol as previously outlined.[33] Cells were carefully seeded onto coverslips and cultured under specific conditions in a controlled environment at 37°C and 5% CO_2. To elicit DNA damage, a defined 6 Gy dose of ionizing radiation was administered to the cells. Following this step, the cells underwent two gentle PBS washes and were subsequently fixed using 4% paraformaldehyde for 10 minutes at room temperature to maintain their structural integrity. The cells were permeabilized using a 0.2% PBS solution with Tween 20 for 10 minutes. Subsequently, to prevent nonspecific binding, the cells were subjected to a 1-hour incubation in a solution of 5% BSA dissolved in PBS. To detect γ-H2AX, an overnight incubation at 4°C was conducted, during which the cells were exposed to an anti-γ-H2AX antibody(9718; CST). Subsequently, the cells underwent incubation with secondary antibodies labeled with fluorochromes, which were sourced from Jackson ImmunoResearch Laboratories. This incubation was carried out for 1 hour at room temperature. To mount the coverslips, ProLong Diamond Antifade reagent, which includes 4′,6-diamidino-2-phenylindole (DAPI) and is provided by Invitrogen, was utilized. Finally, the cells were visualized and staining was analyzed using an immunofluorescence microscope, allowing the acquisition of cell images and the examination of DNA damage markers.

Immunohistochemical analysis

Tumors were fixed overnight at 4°C in 10% phosphate-buffered formalin and embedded in paraffin wax. Sections of 5 μm thickness were cut from the paraffin blocks and mounted on glass slides for immunohistochemical analysis. The sections were permeabilized and blocked to reduce non-specific antibody binding. They were then incubated overnight with anti-γ-H2AX , anti-gp78 and anti-Ki67 antibodies at 4°C, followed by a 30 min incubation with HRP-conjugated secondary antibodies. The antigen-antibody complexes were visualized using a DAB kit.

Ionizing radiation

For ionizing radiation (IR), MDA-MB-231 cells and SUM-159 were exposed to 2.3 Gy/min generated by a 6 MV X-ray linear accelerator (600CD, Varian, USA).

Comet assay

After being exposed to 6 Gy of irradiation, MDA-MB-231 cells were then incubated for the designated period of time. Afterward, the cells were harvested and underwent processing in compliance with the instructions specified by the manufacturer (CometAssay 4250-050-K, Trevigen, Gaithersburg, MD, USA). Briefly, transfecting MDA-MB-231 cells with FLAG-gp78 and control plasmids for 48 hours, the cells were trypsinized and centrifuged. Cells were resuspended in cold PBS at a concentration of 1 × 10^5 cells/mL, then mixed with melted LMAgarose at a ratio of 1:10 (v/v), and immediately pipetted 75 μL onto Comet slides. The slides were laid flat in the dark at 4°C for 10 minutes, then immersed in pre-cooled lysis solution and placed on ice for 30 minutes. Excess buffer was removed from the slides, which were then immersed in freshly prepared alkaline solution. Comet slides were left at room temperature in the alkaline solution for 30 minutes, followed by transfer to a horizontal electrophoresis unit for TBE electrophoresis. After drying, 100 μL of diluted staining solution was applied to each dried agarose circle and allowed to stain in the dark for 30 minutes. Images were captured using fluorescence microscopy, and data were analyzed using CometScore.

HR reporter assay

HR reporter assay was conducted following a protocol as previously documented.[34] DR-GFP -U2OS (HR) cells, containing a single copy of a DR-GFP reporter gene integrated into the genome were used for DSB repair assays. DR-GFP U2OS cells were transfected with FLAG-gp78 and control plasmids for 24 hours. Then, transfection with the I-SceI plasmid to induce DNA damage. After 48 hours post-transfection, cells were harvested, fixed with 10% formaldehyde, washed, and subjected to FACS analysis to determine the proportion of GFP-positive cells.

LC–MS/MS analysis

Cell lysates from MDA-MB-231 cells transfected with FLAG-tagged gp78 were subjected to anti-FLAG-conjugated bead incubation. The immunoprecipitated proteins underwent SDS–PAGE separation and Coomassie Brilliant Blue dye staining. Following excision of protein bands, trypsin buffer digestion was performed for 16 hours at 37°C. Subsequently, the resulting peptides were analyzed using an ultra-high performance liquid chromatography system (AMR) coupled with an Orbitrap Q Exactive mass spectrometer (Thermo Fisher Scientific). Raw data processing, including the generation of extracted ion chromatograms, was accomplished using Sequest and Proteome Discoverer software (Thermo Scientific), with direct analysis conducted using Proteome Discoverer (APPLIED PROTEIN TECHNOLOGY, China).

QUANTIFICATION AND STATISTICAL ANALYSIS

The results are presented as the means ± standard error of the means (SEMs). For comparisons between two groups, statistical analysis was carried out employing unpaired two-tailed Student's t-test, while Comparisons among more than two groups were made using one-way ANOVA. Statistical significance was defined by a P-value threshold below 0.05.